Physico-Chemical Modeling of a Lithium-Ion Battery: An Ageing Study with Electrochemical Impedance Spectroscopy

Marco Heinrich+,[a, b, c] Nicolas Wolff+,[b, c] Nina Harting,[b, c] Vincent Laue,[b, c] Fridolin Röder,[b, c] Steffen Seitz,[a, c] and Ulrike Krewer*[b, c]

Electrochemical Impedance Spectroscopy measurements and simulations are performed on a nickel manganese cobalt oxide (NMC)/graphite pouch cell. A physico-chemical continuum battery model is extended by a physical ageing model including a Solid Electrolyte Interphase. The model assumes a loss of electrochemically active surface area at anode and cathode as well as a growth of solid electrolyte interphase (SEI) layer thickness. These ageing parameters have been adjusted with an algorithm to achieve agreement between simulated and measured spectra. The results for a 28 mAh pouch cell show that the ageing model is suitable to correlate the change of the impedance spectrum with the degree of degradation of the cell. In detail, SEI thickness is shown to increase by 45 nm, while the anode and cathode loose 20% and 57% of their electrochemically active surface area, respectively. In addition, deviating measurement conditions and the end of life of the cell can be indicated by the parameter identification algorithm. Furthermore, it is demonstrated, that the change of the high and low frequency semicircles can be assigned to the anode SEI and cathode respectively.

1. Introduction

Due to their high energy density, lithium-ion batteries (LIBs) have a wide field of application as energy storage technologies and therefore have challenged many research groups to improve performance and to overcome current limitations. Efforts have been undertaken to increase the understanding of degradation processes to be able to increase the cells durability and long-term stability. Another key aspect is to know or at least to predict the end of life (EOL) of cells in use. In most LIBs graphite is used as anode material since its redox potential versus Li+/Li as well as its costs are low. The electrolyte is operated outside its electrochemical stability window and it is therefore being reduced at the anode during cycling. The reduction reaction leads to the growth of a passivating solid electrolyte interphase (SEI) on the anode particles which protects the electrolyte from further reduction. This SEI is believed to be the dominating effect for an increase of cell impedance and a loss of capacity.[1] Therefore, most research neglects all other degradation processes and focuses on the impact of the SEI. Electrochemical impedance spectroscopy (EIS), as a widely used technique to characterise electrochemical systems, is able to reveal ageing induced changes. If processes with different time constants are affected by ageing, they can be revealed at their characteristic frequencies in the impedance spectrum. Impedance spectra of LIBs usually show one or two semicircles in the Nyquist plot. The semicircle with the smaller time constant is often assigned to processes in the SEI and the semicircle with the larger time constant to the charge transfer reactions in anode and cathode.[2] Non-linear frequency response is a further dynamic analysis method yielding complementary helpful insight into the battery state, i.e. state of charge (SoC) and degradation.[3] However, interpretation of resulting spectra is more challenging than in EIS due to the lack of experience. Model-based analysis is presently used to reveal the impact of cell design parameters on such spectra.[4]

In order to gain deeper insight into the processes using EIS, two different types of model approaches are encountered in literature: on the one hand equivalent circuit models (ECMs), and on the other hand continuum models based on physicochemical equations. ECMs need low computational effort and can easily be used to fit simulations to measurement results, which enables an immediate parameter estimation. Nevertheless, ECMs are ambiguous in the assignment of electric circuit components to physical processes as they are phenomenological, empirical models. Continuum models are a more powerful and more physical alternative to get deeper insight into the cell. Also, physics-based models are less prone to overfitting than ECMs, which is a crucial advantage for parameter identifications, as conducted in this work. Doyle et al.[5] have been the first to introduce a continuum model, known as the

[a] *M. Heinrich,+ Dr. S. Seitz*
Physikalisch Technische Bundesanstalt
Bundesallee 100, 38116 Braunschweig, Germany
[b] *M. Heinrich,+ N. Wolff,+ N. Harting, V. Laue, F. Röder, Prof. U. Krewer*
Institute of Energy and Process Systems Engineering
TU Braunschweig
38106 Braunschweig, Germany
Fax: +49 (0)531 391 5932
E mail: u.krewer@tu braunschweig.de
[c] *M. Heinrich,+ N. Wolff,+ N. Harting, V. Laue, F. Röder, Dr. S. Seitz,*
Prof. U. Krewer
Battery Lab Factory
TU Braunschweig
Langer Kamp 8, 38106 Braunschweig, Germany
[+] *These authors contributed equally.*

Newman-model, based on the theories of porous electrode sand concentrated solutions. In order to simulate the EIS of such a physicochemical model, the charging and discharging of double layers has to be included. This has been implemented by Ong et al.[6] and later by Legrand et al.[7]

To analyse ageing phenomena, such models need to be extended by an ageing model including a SEI that accounts for changes due to ageing. Most of the following works though do not analyse the ageing impact on the impedance spectrum. The common assumption that the SEI consists of a dense inner and a porous outer layer is based on the work of Peled et al.[8] in which the physical properties of the SEI are explained. Further, Peled et al.[8] achieved agreement between measured impedance results and an ECM. Based on this work, Gao et al.[9] used a Point Defect Model (PDM) which has been introduced by Macdonald[10] to describe transport processes within the SEI. Using this PDM, Gao has been able to simulate the influence of the SEI on metal surfaces on the impedance spectrum. In order to further analyse the SEI, Nainville et al.[11] developed a model which simulates the growth of the SEI on Lithium anodes. The model does not lead to a quantitative comparison with any experimental results but describes the early growth of the SEI. Broussely et al.[12] extended the prior model and used a full Lithium-ion battery model focusing on calendar ageing. The work of Nainville and Broussely revealed how to store batteries with a minimum of capacity loss. In 2004, Christensen et al.[13] published results for the growth of the SEI at various states of charge with an isothermal physics-based calendar ageing model. At the same time, Ramadass and Ning introduced and applied the currently used model to simulate the growth of the SEI during cyclic ageing.[14–16] Based on the model introduced by Christensen, Colclasure et al.[17,18] developed a thermodynamically consistent model considering the detailed chemistry of the SEI growth for a Single Particle (SP) model of the anode. This approach has been used by Röder who combined it with a kinetic Monte Carlo model to perform multi-scale simulations of the SEI formation.[19] Zavalis did not use a detailed model like Christensen and Colclasure but achieved agreement between simulations and measurement data during ageing.[20] In one of the few works including a model-based analysis of the ageing impact on the impedance spectrum, Xie et al.[21] adjusted simulation parameters of a battery model to investigate impedance data from cycle-aged coin cells. For their research Xie et al.[21] used the model for the SEI growth introduced by Ramadass et al.[14,15] which does not include any transport phenomena nor any reactions within the SEI during an impedance simulation. The current research either focuses on the growth of the SEI and the transport processes within it or on the analysis of the change of battery parameters during ageing using the EIS. A detailed model-based study of the ageing dependent processes at the SEI using impedance spectroscopy will combine the deep insights obtainable from both, physical modelling and EIS. To the authors best knowledge, we here present the first such study.

In this work, we aim to determine and monitor ageing processes by applying a parameter identification (PI) algorithm with ageing-correlated parameters in order to correlate an exemplary set of measurement data at different states of health (SoH) of an in-house made battery cell with the simulation results. We use the detailed thermodynamic approach introduced by Colclasure[17] and focus on the altering influence of the SEI on the impedance spectrum instead on the growth process itself. In contrast to the model presented by Colclasure, we use a full cell SP model with simplifications in the amount of considered reactions and neglect diffusion processes in the SEI. Further, instead of using a side reaction current for the SEI growth, we introduce and apply an ageing model, in order to identify the progression of cell and ageing parameters with time, using EIS. Our model includes a double layer at the SEI/electrolyte interface in addition to the double layer at the particle/SEI interface. The reactions, taking place at those interfaces, are coupled which is a drastic change compared to equivalent circuit modelling, where the impedance of each process is independent of every other process. Further, the loss of lithium during the formation and the loss of active material due to particle cracking and due to a loss of connectivity between the active materials and the current collectors are implemented. Both losses are assumed to change the allocation of lithium in anode and cathode. Therefore, the SoC changes and the resulting impedance spectrum is affected. In addition to that, the isolating effect of the SEI is considered in the model. We present the first impedance simulations on such a model and show that the model is suitable to provide detailed information on the change of ageing parameters during degradation and enabling a physical-based interpretation of this change. This approach enables a state estimation at various states of health and it might also be suitable to indicate the EOL of the cell. The focus of this work lies in the implementation of the new ageing model including the state estimation of an exemplary chosen cell. Validation of the model with various cycling conditions or predicting the exact capacity after a specific amount of cycles is open for future research. Nevertheless, we show that our method provides a significant improvement to the classical analysis of impedance and capacity values.

2. Modeling

A SP full cell battery model including a SEI (SP-SEI) at the anode side, schematically shown in Figure 1, is derived in this section. The geometry underlying the model is illustrated in Figure 1. It consists of a negative electrode, a positive electrode and a separator in between. Both electrodes are assumed to be porous. Electrodes and separator are not discretised in x-direction for this study to focus on the analysis of the main effects. Modelled spherical active material particles are radially discretised. On the anode side, an additional SEI layer is implemented as shown in Figure 1b.[22] During the charging process a solvated Lithium-ion, originating from the electrolyte phase, enters the interfacial area (IFA) between liquid electrolyte and solid electrolyte, where it loses its solvate layer. This process is analogously described to a charge transfer reaction and is displayed in Figure 1c as a potential drop. Next to the

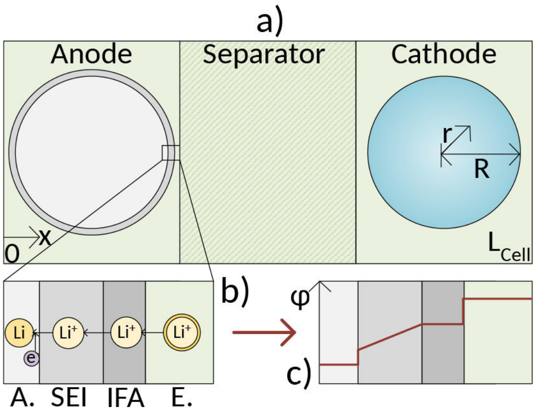

Figure 1. a) SP battery model including b) a magnified illustration of the anode particle/SEI/electrolyte interface region and c) the corresponding potential distribution.

interfacial area, the SEI is present and an Ohmic potential distribution causing a linear potential drop is assumed. At the particle-SEI interface, Lithium electrochemically reacts and intercalates in a next step into the active material particle. The IFA, in contrary to the SEI, is not modelled with a dimension in x-direction since it is included in order to calculate the adsorption process only. Therefore the IFA does not have a thickness.

2.1. Single Particle Model

The phenomenon of solid state diffusion within active material particles is described by Fick's second law. It is formulated using radial coordinates with the radius r to account for the spherical shape of the active material particles.

$$\frac{\partial c_s}{\partial t} = \frac{1}{r^2}\frac{\partial}{\partial r}\left(D_s r^2 \frac{\partial c_s}{\partial r}\right) \tag{1}$$

Using c_s as solid concentration and D_s as solid Diffusion coefficient. At the center of the particle, $r = 0$, the concentration gradient is set to zero. The flux across the outer particle boundary, $r = R$, is set to the Lithium-ion reaction flux j_{Li}.

The charge flux J_k, by the species $k = \{Li^+, PF_6^-\}$, is calculated with a Nernst-Planck flux, with the convection term set to zero:

$$J_k = \underbrace{D_k \frac{\partial c_k}{\partial x}}_{\text{Diffusion}} + \underbrace{D_k^{\mathrm{mig}} \frac{\partial \Phi}{\partial x}}_{\text{Migration}}, \tag{2}$$

with the potential Φ and the potential induced transport coefficient D_k^{mig}:

$$D_k^{\mathrm{mig}} = \frac{z_k F c_k(x,t) D_k}{\mathrm{R}T}, \tag{3}$$

with the valence of ions z_k, the Faraday constant F, the gas constant R and the cell temperature T. Combining Equation 2 with the continuity equation

$$\frac{\partial c_k}{\partial t} = \quad \frac{\partial J_k}{\partial x}, \tag{4}$$

leads to a material balance equation for the species concentration c_k with $k = \{Li^+, PF_6^-\}$ in the bulk of the electrolyte:

$$\frac{\partial c_k}{\partial t} = \frac{\partial}{\partial x}\left(D_k \frac{\partial c_k}{\partial x}\right) + \frac{\partial}{\partial x}\left(D_k^{\mathrm{mig}} \frac{\partial \Phi}{\partial x}\right) \tag{5}$$

A system with two oppositely charged species Li^+ and PF_6^- is present. Since electroneutrality $\sum z_k c_k = 0$ within the electrolyte is assumed, c_{Li^+} and c_{PF_6} are equal and the migration term cancels out.[23] To consider the effect of the Lithium reaction, a source term is added, which couples the equations for solid and electrolyte diffusion. Therefore, the overall change in electrolyte concentration c_e is provided by the material balance in Equation 6.

$$\frac{\partial c_e}{\partial t} = D_e \frac{\partial^2 c_e}{\partial x^2} + (1 \quad t_p)\frac{j_{\mathrm{Li},m}}{F}, \tag{6}$$

with $m = \{\mathrm{c}, \mathrm{a}\}$ for cathode and anode respectively. A concentration gradient of zero is assumed at $x = \{0, L_{\mathrm{cell}}\}$. The electrolyte diffusion coefficient D_e and the transference number t_p are being calculated as:[5]

$$D_e = \frac{2D_{\mathrm{Li}} + D_{\mathrm{PF}_6}}{D_{\mathrm{Li}+} + D_{\mathrm{PF}_6}}, \tag{7}$$

$$t_p = \frac{D_{\mathrm{Li}^+}}{D_{\mathrm{PF}_6} + D_{\mathrm{Li}^+}}, \tag{8}$$

with the Diffusion coefficients of positively D_{Li^+} and negatively D_{PF_6} charged species.

The flux of Lithium-ions $j_{\mathrm{Li,c}}$ at the cathode side in Equation 6 is calculated with the Butler-Volmer equation.

$$j_{\mathrm{Li,c}} = a_{\mathrm{s,c}} j_{0,\mathrm{c}}\left(\exp\left(\alpha_{\mathrm{c}}\tfrac{\eta_{\mathrm{c}}\mathrm{F}}{\mathrm{R}T}\right) \quad \exp\left(\left((1 \quad \alpha_{\mathrm{c}})\tfrac{\eta_{\mathrm{c}}\mathrm{F}}{\mathrm{R}T}\right)\right)\right), \tag{9}$$

with the cathode reaction symmetry factor α_c, the overpotential η_c and the specific surface area $a_{s,c}$, which is defined as,

$$a_{\mathrm{s,m}} = \frac{3\varepsilon_{\mathrm{s,m}}}{R}, \tag{10}$$

with the solid phase volume fraction ε_s and the particle radius R.

A concentration dependent exchange current density $j_{0,c}$ is implemented with respect to the maximum concentration in the cathode $c_{\mathrm{max,c}}$.[17]

$$j_{0,\mathrm{c}} = k_{\mathrm{c}} \mathrm{F} c_e^{\alpha}\left(c_{\mathrm{max,c}} \quad c_{\mathrm{s,c}}\right)^{\alpha} c_{\mathrm{s,c}}^{1-\alpha}, \tag{11}$$

with k_c as the reaction rate constant, $c_{s,c}$ as the concentration in the cathode and c_e as Lithium concentration in the electrolyte.

At the interfaces between anode/SEI, electrolyte/SEI and cathode/electrolyte, shown in Figure 1, the overall current splits up into a reaction current $j_{\mathrm{Li},i}$ and a double layer charge current $j_{\mathrm{DL},i}$. Therefore, additionally to the reaction flux, defined in Equation 9, a flux into the double layer has to be calculated.

$$j_{\mathrm{DL},i} = a_{\mathrm{s,i}} C^{\mathrm{DL}_i} \frac{\partial \Delta\Phi_i}{\partial t}, \tag{12}$$

with C^{DL} as the active material area-related double layer capacitance and $\Delta\Phi$ as the potential difference between the two phases. The time derivation is causing a phase shift between current and voltage which leads to the imaginary parts in the impedance.

2.2. Implementation of the SEI

At the anode side of the model, a SEI is implemented. The entering of Lithium-ions into the interfacial area between solid and liquid electrolyte might be closely related to the skimming of their solvate layer.[24] Yamada et al.[25] reported that this might be the rate-determining step, but no further research on this topic has been reported yet. The reaction can be described as:

$$\mathrm{Li}^{+} + V_{\mathrm{Li}} \rightleftharpoons \mathrm{Li}^{+}_{\mathrm{IFA}}, \tag{13}$$

with V_{Li} as vacancies at the IFA.[17] Afterwards the Lithium-ions enter the SEI from the IFA.

$$\mathrm{Li}^{+}_{\mathrm{IFA}} \rightleftharpoons \mathrm{Li}^{+}_{\mathrm{SEI}} + V_{\mathrm{Li}} \tag{14}$$

This reaction is directly coupled with a charge-transfer reaction at the SEI/particle interface to enforce charge neutrality within the SEI.

$$\mathrm{Li}^{+} + e^{-} \rightleftharpoons \mathrm{Li} \tag{15}$$

The ion flux resulting from these coupled processes is calculated with Equation 16 according to,[26]

$$j_{\mathrm{Li,a}} = \frac{c_{\mathrm{Li,a}} \gamma_{\mathrm{Li}} \lambda_{\mathrm{a,SEI}} \lambda_{\mathrm{SEI,IFA}} \quad c_{\mathrm{Li,IFA}} \gamma_{\mathrm{V}} \lambda_{\mathrm{SEI,a}} \lambda_{\mathrm{IFA,SEI}}}{\lambda_{\mathrm{SEI,a}} + \lambda_{\mathrm{SEI,IFA}}}, \tag{16}$$

with $c_{\mathrm{Li,IFA}}$ as Lithium-ion concentration at the interfacial area, $c_{\mathrm{Li,a}}$ as Lithium concentration at the surface of the active material particle and $j_{\mathrm{Li,a}}$ as the volume specific current generated by the coupled reactions 14 and 15. The activity coefficients of the Lithium γ_{Li} and the vacancies γ_{V} are calculated using a Redlich-Kister approach according to:[17]

$$\gamma_{\mathrm{Li}} = \exp \quad \frac{1}{\mathrm{R}T}(1 \quad y_{\mathrm{a}})^2 \sum_{i \; 1}^{11} A_i \, (2y_{\mathrm{a}} \quad 1)^i \left(1 + \frac{2iy_{\mathrm{a}}}{2y_{\mathrm{a}} \quad 1}\right)\Bigg), \tag{17}$$

$$\gamma_{\mathrm{V}} = \exp \quad \frac{1}{\mathrm{R}T} y_{\mathrm{a}}^2 \sum_{i \; 1}^{11} A_i (2y_a \quad 1)^i \left(1 + \frac{2i(1 \quad y_{\mathrm{a}})}{2y_{\mathrm{a}} \quad 1}\right)\Bigg), \tag{18}$$

with $y_{\mathrm{a}} = c_{\mathrm{a}}/c_{\mathrm{max,a}}$ and A_i as Redlich-Kister parameters, which are listed in the experimental section in Table 4. To solve Equation 16, the reaction coefficients $\lambda_{\mathrm{a,SEI}}$, $\lambda_{\mathrm{SEI,a}}$, $\lambda_{\mathrm{SEI,IFA}}$ and $\lambda_{\mathrm{IFA,SEI}}$ are needed. The index a, SEI equals the forward and the index SEI, a the backwards main charge transfer reaction. The indices SEI, IFA and IFA, SEI are used in the same manner for the concentration dependent reaction. We assume the following reaction kinetics:

$$\lambda_{a,SEI} = a_{s,a} \cdot k_{f,a} \exp\left(\alpha_a \Delta\Phi_a \frac{\mathrm{F}}{\mathrm{R}T}\right), \tag{19}$$

$$\lambda_{SEI,a} = a_{s,a} \cdot k_{b,a} \cdot \exp\left(\quad (1 \quad \alpha_a)\Delta\Phi_a \frac{\mathrm{F}}{\mathrm{R}T}\right), \tag{20}$$

$$\lambda_{SEI,IFA} = a_{s,IFA} \cdot k_{f,SEI} \cdot \Theta_v, \tag{21}$$

$$\lambda_{IFA,SEI} = a_{s,IFA} \cdot k_{b,SEI}, \tag{22}$$

with the reaction rate constants $k_{f,a}$, $k_{b,a}$, $k_{f,SEI}$ and $k_{b,SEI}$ for each forward and backward reaction, α_a as reaction symmetry factor and with the vacant surface sites Θ_v.

The ion flux generated from the reaction in Equation 13 can be expressed with the following equations by introducing the fraction of surface sites occupied by Lithium ions Θ_{Li}.

$$\begin{aligned} j_{\mathrm{Li,IFA}} &= \mathit{\Theta}_v \cdot \alpha_{\mathrm{s,IFA}} \cdot c_{\mathrm{Li,e}} \cdot k_{\mathrm{b,IFA}} \exp\left(\quad (1 \quad \beta)\Delta\Phi)\frac{\mathrm{F}}{RT}\right) \\ &\quad \Theta_{\mathrm{Li}} \cdot a_{\mathrm{s,IFA}} \cdot k_{\mathrm{f,IFA}} \exp\left(\beta\Delta\Phi \frac{\mathrm{F}}{\mathrm{R}T}\right) \end{aligned} \tag{23}$$

We are aware of the fact, that the reaction might not be exponentially dependent on the overpotential but linear dependent instead, but for impedance simulations no significant change in the results can occur since the excitation has to lead to a linear system response anyway. The assumption of an exponential potential depended transport of charged species from the liquid electrolyte to the solid electrolyte is based on the results presented by Kitazumi et al.[27]

2.3. Ageing Model

During ageing, the internal resistance of the cell increases. In order to account for this increase, the SEI thickness d_{SEI} is assumed to cause a potential drop which is dependent on the conductivity σ_{SEI}:

$$\Delta\Phi_{\mathrm{SEI}} = \frac{d_{\mathrm{SEI}}}{\sigma_{\mathrm{SEI}}} J_{\mathrm{Li}} \tag{24}$$

The initial thickness of the SEI, which is formed during the formation of the battery, is calculated according to:

$$d_{\mathrm{SEI,init}} = \frac{V_{\mathrm{SEI}} R_{\mathrm{a}}}{3\varepsilon_{\mathrm{s,a}} A_{\mathrm{cell}} d_{\mathrm{a}}} \tag{25}$$

We use the assumption, that 15% of the Lithium, which deintercalates the cathode during the first charge will build up an initial SEI in the formation process instead of intercalating into the anode.[28] This initial SEI is assumed to be composed of pure Lithium carbonate.

$$V_{\mathrm{SEI}} = \frac{n_{\mathrm{loss}} M_{\mathrm{Li_2CO_3}}}{2\rho_{\mathrm{Li_2CO_3}}}, \tag{26}$$

with the amount of lost mol Lithium n_{loss} and the molar mass and density of Lithium carbonate $M_{\mathrm{Li_2CO_3}}$ and $\rho_{\mathrm{Li_2CO_3}}$ respectively. The capacity decrease of the cell during cycling is accounted for by a loss of active material in anode and cathode of equal amount corresponding to a loss in active material fraction $\varepsilon_{\mathrm{loss}}$ at anode and cathode.

$$\varepsilon_{\mathrm{s,a,age}} = \varepsilon_{\mathrm{s,a}} - \varepsilon_{\mathrm{loss}}, \tag{27}$$

$$\varepsilon_{\mathrm{s,c,age}} = \varepsilon_{\mathrm{s,c}} - \varepsilon_{\mathrm{loss}}, \tag{28}$$

with the solid phase volume fraction after ageing $\varepsilon_{\mathrm{s,age}}$ and the lost solid phase volume fraction $\varepsilon_{\mathrm{loss}}$. Due to the loss of active material the SoC of the cell is affected. This has been accounted for by simulating one charge/discharge routine with the new amount of active material in order to set the initial values of the state variables at the shifted SoC 50.

Additionally to an increased SEI thickness and to the loss of a certain fraction of active material, ageing is assumed to affect the electrochemical reactions as well as the corresponding double layers. Reaction products can decrease the micro-porosity[29] and the loss of active material reduces the surface available for reaction. Surface film formation and further mechanical and chemical degradation of particles causes electrical isolation of particles[30] at anode and cathode, thereby influencing the active surface areas $a_{\mathrm{s,m}}$[31] and therefore the reaction overpotentials. Due to this electrical isolation the charge transfer process is affected in any case while different scenarios are tested in order to find out if the corresponding double layer is affected as well. The priorly described ageing principle is illustrated in Figure 2 for the isolations at the anode interfaces. Depicted is an example, where the double layer of the first interface is affected while the double layer of the second interface is unaffected by the isolation. Within the SP model, the isolations are mathematically accounted for with isolations p_{a}, p_{IFA} and p_{c}, reducing the corresponding specific surface areas of the anode/SEI $a_{\mathrm{s,a,age}}$, the IFA/electrolyte $a_{\mathrm{s,IFA,age}}$ and the cathode/electrolyte interfaces:

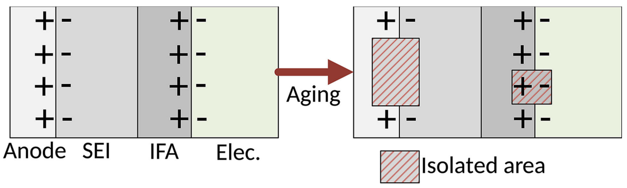

Figure 2. Schematic illustration of the ageing induced isolation exemplary shown at the two anode interfaces. The reaction is being blocked at both interfaces. At the inner interface charges are shifted by the isolation as well, which affects the related double layer.

$$a_{\mathrm{s,a,age}} = a_{\mathrm{s,a}} \cdot (1 - p_{\mathrm{a}}), \tag{29}$$

$$a_{\mathrm{s,IFA,age}} = a_{\mathrm{s,IFA}} \cdot (1 - p_{\mathrm{IFA}}) \tag{30}$$

$$a_{\mathrm{s,c,age}} = a_{\mathrm{s,c}} \cdot (1 - p_{\mathrm{c}}) \tag{31}$$

The complete introduced ageing model includes several assumptions. Although, all of these assumptions are based on physical processes which have been reported for the ageing of Lithium-ion batteries in previous research, cross validation of the model to proof all assumptions is beyond the scope of this research. The focus of this work is set on a state estimation of one cell at different SoHs in order to show the applicability and the current limits of the model.

2.4. PI Algorithm

PI is conducted using a non-linear least square trust-region-reflective algorithm embedded in Matlab. The objective function $\chi^2(\omega, \theta)$, shown in Equation 32, contains the relative error for the real part of the measurement and simulation for the investigated frequencies ω_i of the part of the spectrum which is fitted. Using the real part of the impedance for the objective function was found to lead to better results than using an objective function combined of real and imaginary part or combined of phase and impedance. This is because of the use of a SP-model instead of a more discretised model. A SP-model calculates a defined deviation of the imaginary part of the impedance to the measured semicircles, since it calculates one perfect charge transfer process on each electrode, whereas e.g. a pseudo-two-dimensional (P2D) model or a model including a particle size distribution (PSD) simulate one charge transfer process for each modelled particle. If the charge transfer processes in such a model occur at different time constants, e.g. due to different local overpotentials for each particle, the resulting semicircle in the Nyquist plot will be flattened, while semicircles simulated on a SP model are always unmodified. It should be noted at this point that using a P2D model does not lead to a distribution of time constants similar to the actual one in the cell. This can be seen in the results presented by Tippmann et al.[32] The usage of a model including a PSD would be a significant improvement but as long as the actual charge distribution within the cell is unknown the model includes an epistemic uncertainty. Since the described deviation is not physic-based but model-based, including the imaginary part or the phase of the impedance in the objective function will decrease the quality of the result. Thus, using the real part of the impedance avoids over-fitting, as the PI algorithm otherwise would try to fit a feature the model is not capable to simulate. Therefore, the function which the in Matlab implemented Trust Region Reflective Algorithm minimises is:

$$\chi(\omega, \theta) = \min \sum_{i}^{k} \left| \frac{Re_{\mathrm{meas}}^{\omega_i} - Re_{\mathrm{sim}}^{\omega_i}}{Re_{\mathrm{meas}}^{\omega_i}} \right|^2 \tag{32}$$

θ represents the parameters to be identified and k the number of frequencies. Since the real part and imaginary part of the impedance are correlated by the Kramers-Kronig relations the results of the parameter identification still include an error due to the use of the single particle model.

3. Results and Discussion

This section starts by discussing the EIS and capacity measurements. In the second part, the parameters of the unaged cell are identified and discussed. Afterwards, the ageing model is applied to investigate the change of the cell impedance during ageing. Finally, the ageing progress is discussed based on the evolution of ageing parameters during cycling. Matlab has been used to perform the simulations in time domain.

3.1. Measurement Results

In Figure 3, the impedance spectra of the cycle-aged cell are shown in a Nyquist plot. At very high frequencies the system shows inductive behaviour which is induced by the wiring and not by the battery. Therefore, the inductive behaviour is not included in the model. The intersection of the measurement with the x-axis at high frequencies is magnified in the inset. The corresponding real part is assigned to the internal resistance of the cell and increases monotonously with increasing cycling number. In the frequency range from 0.3 Hz to 205 kHz, two semicircles are visible. The left and bigger one has a maximum imaginary part at 1.4 kHz and is attributed to the SEI, whereas the smaller one with a characteristic frequency of 7.2 Hz is attributed to the charge transfer reactions in anode and cathode.[2] During cyclic ageing the characteristic frequency of the SEI semicircle shifts from 1.4 kHz at the BOL to 1 kHz after 350 cycles while the characteristic frequency of the charge transfer reaction shifts from 7.2 Hz at the BOL to 2 Hz after 350 cycles. This indicates that both related processes decelerate due to the ageing of the cell. Next to the low frequency semicircle, in the low frequency range, the impedance rises linearly, as it is characteristic for semi-infinite diffusion processes. It is attributed to solid diffusion in the active material particles. Furthermore, with increasing cycle number, the spectra shift to higher real parts of the impedance due to an increase of the internal resistance of the cell. Moreover, the semicircle of the SEI as well as the semicircle of the charge transfer reactions widen. The general trend of increasing impedances, visible in Figure 3, which leads to a widening of the semicircles and to a right shift of the spectrum, has been reported in literature before.[21]

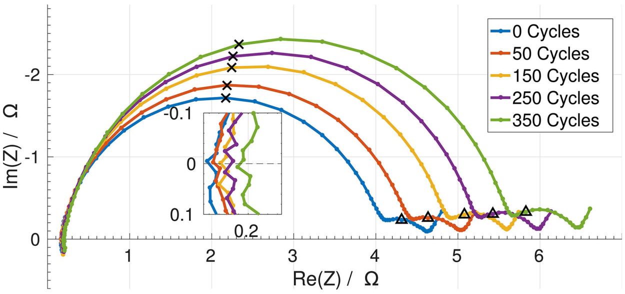

Figure 3. EIS measurements for a cycle aged Lithium ion battery at SoC 50 %. × and Δ indicate impedance points at 1.4 kHz and 7.2 Hz respectively.

In addition to the Nyquist plots in Figure 3, the capacity fade and the impedance at the characteristic frequencies of the semicircles are displayed in Figure 4. Within the first 350 cycles, the SoH decreases from 100 % to 83.33 %. During the last measured 50 cycles, the capacity decreases drastically by additional 73.5 %, indicating the EOL of the battery. The red graphs in Figure 4 show the absolute values of the impedance at the characteristic frequencies of the two semicircles with increasing cycle number. Both impedances increase monotonously during the first 350 cycles due to the proceeding ageing of the cell. The increase at 7.2 Hz is more distinct because the impedance at lower frequencies includes the response of all faster processes whereas at high frequencies, the slower processes are not excited by the sinusoidal input. Therefore, at 7.2 Hz charge transfer and SEI influence is visible while at 1.4 kHz the impedance is only influenced by the internal resistance and the SEI. The measurement results further show, for example within the first 100 cycles, that the loss of capacity can not be correlated with the impedance of the cell. For the first 50 cycles almost no loss of capacity has been measured while the impedance of the cell rises. During the next 50 cycles the SoH decreases more noticeable while the impedance rise is a bit lower.

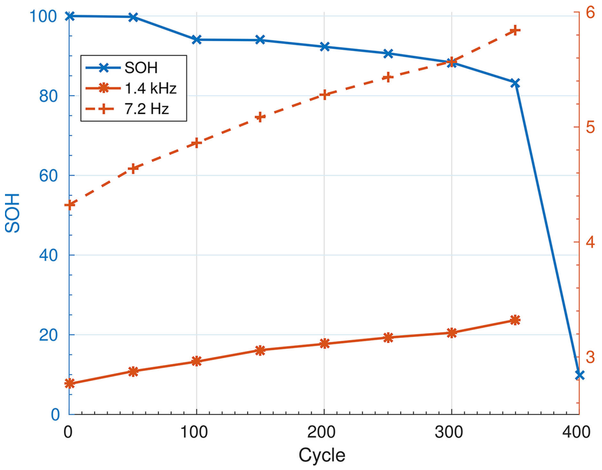

Figure 4. The State of Health (blue) and the impedances (red) at 7.2 Hz (dashed) and 1.4 kHz (solid) for the cycled battery.

3.2. Identification of Kinetic Parameters

In a next step, kinetic and transport parameters of the model are identified using the parameters presented in Table 3 and the impedance measurement of the unaged cell. This step is performed prior to the analysis of the degradation in order to determine the unknown reaction rate constants k_{SEI}, k_c and k_{IFA} as well as the corresponding double layer capacitances C_a^{DL}, C_c^{DL} and $C_{\mathrm{IFA}}^{\mathrm{DL}}$. Additionally, the thickness of the initial SEI $d_{\mathrm{SEI,init}}$ and the conductivity of the SEI σ_{SEI} are identified. The PI is performed sequentially in order to decrease the simulation time and to ensure uniqueness of the fit. For a detailed investigation of the limitation of parameter estimation from EIS data the reader is referred to the work of Alavi et al.[33] Since parameters affect only a specific time constant of the spectrum, PI can be performed beginning from highfrequencies to low frequencies without loss of accuracy. First, the volume of the initial SEI and the related thickness of the SEI are calculated with Equations 25 and 26, givinga value of $d_{\mathrm{SEI,init}} = 184$ nm. The calculated value is higher than the reported values from Christensen[13] because we calculated the thickness from the Lithium being lost during the first cycles, while Christensen used reaction kinetics to determine the thickness. Our result is strongly dependent on the assumption for the amount of Lithium being lost and on the material parameters of the SEI. In general, values for the thickness of the SEI reported in literature vary strongly which aggravates comparison. After determining the initial SEI thickness in a first step, the internal resistance of the cell is identified by adjusting the conductivity of the SEI σ_{SEI}. Afterwards, the high frequency semicircle is adjusted by identifying k_{tIFA} and $C_{\mathrm{tIFA}}^{\mathrm{DL}}$. The last step includes the identification of k_{SEI}, k_c, C_a^{DL} and C_c^{DL} with the impedance data from the low frequency semicircle. Since the coupled anode reactions are linked with the reaction at the interfacial area by the free surface sites on the IFA, the related time constant is lower than the time constant of the cathode reaction, which has also been reported by Illig et al.[34] Using this information for the PI at the low frequency semicircle enables unambiguous results with four parameters. The resulting values for the identified parameters are given in Table 1. At the anode side, double layer capacitances at both interfaces of the SEI differ by more than four orders of magnitude with the one at the electrolyte interface being significantly smaller. This discrepancy is reasonable since the related measured bigger semicircle has a much smaller time constant and is clearly separated from the low frequency semicircle. The double layer capacitance of the IFA is expectably much smaller than the anode double layer capacitance. In comparison to the capacity values found by Huang et al.[35] the value for the IFA in this work is very small while the identified value for the anode is higher than the one suggested by Huang et al. Additionally, the values presented in the works of Ong,[6] Xie[21] and Tippmann[32] differ not only significantly to our and but also to the values which Huang suggested. Therefore, further research on reliable measurements of the double layer capacitance is needed. For the reaction rate constants at the anode and interfacial area no comparison with literature values is possible since a novel approach to couple the SEI reactions according to Equation 16 is used. The calculated cathode reaction rate constant is in agreement with the value presented by Colclasure et al.[18]

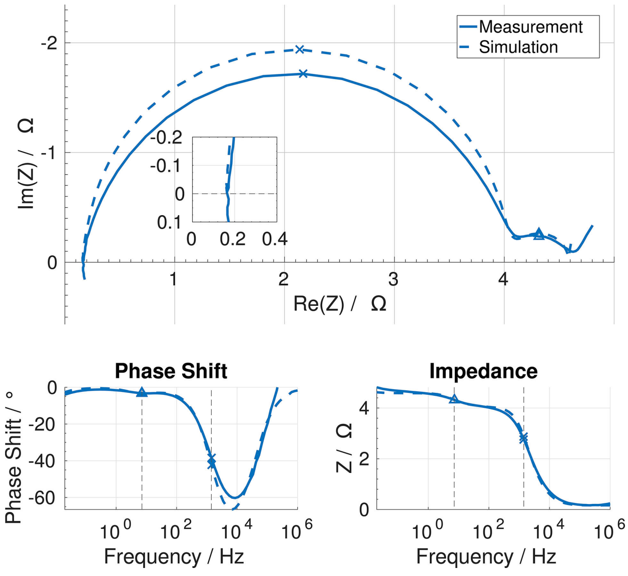

Figure 5. Experimental (solid line) and simulated (dashed line) EIS for an unaged Lithium ion battery at SoC 50 % and T = 25 °C. × and Δ indicate impedance points at 1.4 kHz and 7.2 Hz respectively.

Experiment and the resulting simulated EIS are shown in Figure 5. The simulation matches the internal resistance well but is not able to meet the imaginary part at the peak of the high frequency semicircle as discussed in Section 2.4. The Bode plots confirm this deviation and highlight that phase shift and impedance of the measurement are slightly shifted to higher frequencies in the range of the high frequency semicircle. Using the introduced model, the simulated high frequency semicircle includes only one time constant for the processes at the SEI/electrolyte interface. Therefore, the flattening of the high frequency semicircle can not be reproduced perfectly. The algorithm for the PI is able to reproduce the low frequency semicircle well, since the two characteristic frequencies for the two main charge transfer reactions at anode and cathode are in this frequency range. Another deviation is visible at the diffusion part of the impedance spectrum at low frequencies. Due to the low slope of the anode OCV-curve the anode does not show any diffusion impedance.[34] The remaining cathode diffusion impedance, simulated with a SP model, always increases with a 45° slope, while the measured impedance increases with a higher slope, since multiple diffusion processes with different time constants take place.[36]

3.3. Identification of Ageing Parameters

The ageing process is analysed using the SP-SEI model via identifying changes in the loss of active material $\varepsilon_{\mathrm{loss}}$, the SEI-thickness d_{SEI}, the isolation of the SEI/electrolyte interface p_{IFA}, the isolation of the particle/SEI interface p_a and the isolation of the cathode surface p_c using the observed change in the impedance spectra. Starting from the parameters of the unaged cell, the PI algorithm is applied for every aged impedance spectrum sequentially by extracting the relevant ageing parameters from the capacity and the internal resistance, than from the high frequency semicircle and in the end from the low frequency semicircle. This routine is similar to the one introduced by Zavalis et al.[20] The change of the capacity of the cell during ageing is simulated by a change of the available active material. Therefore, the solid phase volume fraction is reduced following Equation 27. It is assumed that the loss of active material takes place at both electrodes and that the lost active material is fully lithiated, because the mechanical stress within the particles is at a maximum if the maximum possible amount of lithium is intercalated. Then the thickness of the SEI is adjusted to reproduce the experimentally observed change of the internal resistance. Afterwards the isolation at the SEI/electrolyte interface is identified using the high frequency semicircle. Since the time constant of the high frequency semicircle increases during ageing, better agreement with the experiment is achieved when assuming that the related double layer of the SEI/electrolyte interface is unaffected by the isolation. This assumption is physically based on the idea that the absolute value of the double layer might change but not the area weighted value which has been used for the simulations.[20] The resulting increase of the time constant of the high frequency semicircle shifts the time constant of the low frequency semicircle as well, because the related reactions are coupled. For the low frequency semicircle which is characterised by the charge transfer at anode and cathode, several degradation options were evaluated regarding their ability to reproduce the changes in the EIS. In order to determine the physically most reasonable option for the ageing model all possible options are simulated and the results of the PI algorithm are evaluated. The options differ in the interfaces which are isolated and whether the related double layer capacitance is affected by the isolation, using the Equations 29–31, or not. Table 2 shows the normalized residuum of the objective function and the resulting isolations for all twelve model options extracted from the low frequency semicircle after 350 cycles.

Table 1. Model parameters identified using the impedance spectrum measured on the unaged cell.

Parameter	IFA	SEI	Anode	Cathode
Double layer capacitance $C^{\mathrm{DL}}/\frac{F}{m^2}$	$1.75\cdot10^{\ 3}$		17.89	1.70
Reaction rate constant $k_f/\frac{m^{2\ 5}}{mol^{0\ 5}s}$	1.85	$4.99\cdot10^{6}$	Table 3	$2.05\cdot10^{\ 10}$
SEI Conductivity $\sigma_{\mathrm{SEI}}/\frac{S}{m}$		$8.76\cdot10^{\ 5}$		

With Table 2 three options in bold can be identified to produce the best possible agreement with the experimental data. All three options have zero anode isolation. For the first two of these options, both interfaces are affected by isolations. In the last option, the PI algorithm can only adjust the cathode isolation. The second best result was achieved withan isolation on both interfaces which do not affect the related double layer capacitances leading to isolations of 28 % and 43 % for anode and cathode respectively. Since the PI algorithm leads to optimal results for zero anode isolation and to good results with significantly higher cathode isolation, our algorithm clearly suggests, that mainly or only cathode isolation took place as previously shown by Abraham et al.[37,38] The low frequency semicircle changes are thus mainly attributed to an isolation at the cathode. Since the high frequency semicircle is changing its size due to an isolation at the SEI/electrolyte interface as discussed previously, the results point out that the change of the high and low frequency semicircles can be referred to degradation at the anode and cathode respectively. Furthermore, the high frequency semicircle is influenced by degradation at the SEI/electrolyte interface, while the low frequency semicircle is affected by degradation at the cathode/electrolyte interface. As such our model-based analysis suggest that the two interfaces facing the electrolyte are being isolated during ageing and thus affecting the impedance spectrum, while the electrode/SEI interface has a negligible impact.

Using the above described sequentially applied parameter identification with the chosen model options leads to the results presented in Figure 6. It shows that the applied ageing model can reproduce the experimentally observed ageing effects on the EIS. The simulation results for the Nyquist and Bode plots, displayed as dotted lines, are in a good agreement with the solid lines representing the measurement results. The widening of the two semicircle, as well as the increase of the internal resistance, is indeed reproduced very accurately. However, for the low frequency semicircle, it can be seen that reproduction of the experiment by the model decreases with increasing cycle number, while the differences of the impedance between measurement and simulation at the high frequency semicircle are not higher than for the previous cycles. Considering the fact that the SoH of the cell decreases drastically from 350 cycles to 400 cycles, as presented in Figure 4, we assume that an additional ageing process, e.g. a loss of electrical connectivity between the current collector and the active material, occurs. As the model can not reproduce the effect of this process on the impedance of the system, it seems

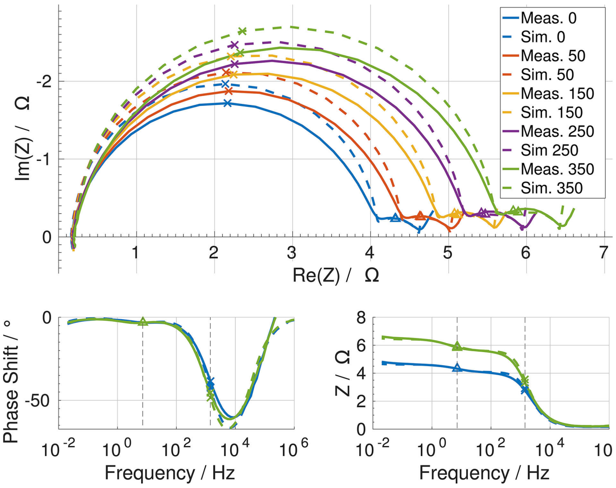

Figure 6. Measured and simulated EIS for the cycling aged Lithium ion battery at SoC 50 % and T = 25 °C. × and Δ indicate impedance points at 1.4 kHz and 7.2 Hz respectively.

Table 2. Impact of the model options on the parameter identification at the low frequency semicircle after 350 cycles. The first value in each cell is the normalized residuum of the objective function. Second and third values show the calculated isolations in percent for anode and cathode, respectively.

affected double layer capacitance	isolated interfaces both electrodes	anode only	cathode only
both electrodes	**$3.52\cdot10^{4}$** **0/57.39**	$2.5\cdot10^{3}$ 21.31/fixed 0	$3.52\cdot10^{4}$ fixed 0/57.39
anode only	$1.2\cdot10^{3}$ 16.49/50.16	$2.5\cdot10^{3}$ 21.31/fixed 0	$3.8\cdot10^{3}$ fixed 0/60.52
cathode only	**$3.52\cdot10^{4}$** **0/57.39**	$1.1\cdot10^{3}$ 34.58/fixed 0	**$3.52\cdot10^{4}$** **fixed 0/57.39**
both DL unaffected	$4.61\cdot10^{4}$ 28.31/43.4	$1.1\cdot10^{3}$ 34.58/fixed 0	$3.8\cdot10^{3}$ fixed 0/60.52

that the occurring ageing process is not included in the model. Since this process only occurs close to the EOL of the cell at 400 cycles, it may well be responsible for the EOL. In this case, the discrepancy between model and experiment may indeed be a good indication for the nearing EOL. As we assigned the change of the low frequency semicircle to degradation processes in the cathode, the results in Figure 6 indicate that the additional ageing process rather affects the cathode than the anode. In conclusion, the occurrence of an undefined, not included ageing phenomenon seems to be detectable with our model and it may allow to predict the EOL.

As the reproduction of the ageing effects on the EIS was successful, this allows to interpret the progression of the underlying ageing parameters with respect to the cycle number herein given in Figure 7. All ageing parameters increase during the cyclic ageing except for the particle/SEI isolation which is zero at all cycles as discussed previously. The increase of the SEI thickness of approximately 50 nm is in agreement with several research results.[13,39–41] Due to Equation 24 which is used to calculate the potential distribution across the SEI, the increasing SEI-thickness accounts for the rise of the internal resistance of the cell during ageing. It should be noted, that the introduced ageing model can overestimate the thickness of the SEI if an increase of the internal resistance is not solely caused by the SEI which is likely to occur at the EOL of the cell. By extending the model with more ageing processes which influence the internal resistance as well, the thickness of the SEI could be determined more precisely. However, a separation of different ohmic loss contributions to the internal resistance is barely possible. Within this research, a model extension, e. g. with a ageing-dependent electrolyte resistance, has not been implemented and the determined values for the SEI-thickness are therefore affected by an epistemic uncertainty. The surface isolation of the SEI/electrolyte interface as well as the thickness of the SEI show a constant increase within the overall cycle range. This monotonous increase occurs in agreement with the capacity loss, the increase of the internal resistance and the monotonously increase of the impedance, shown in Figure 4, during cycling. For the cathode a high degree of isolated area is identified. Analysing the low frequency semicircle shows, that the diameter increases by approximately 57 % during the first 350 cycles. Since the EIS is a linear method, a cathode isolation of 57 % after 350 cycles is therefore consistent if the isolation is the only degradation process, which affects the diameter. In contrast, to adjust the high frequency semicircle, a lower degree of isolated surface area, approximately 20 %, is needed. The high frequency semicircle is bigger than the low frequency semicircle, but its percental change during ageing is lower. To our best knowledge, no values for the surface isolations of the interfaces have been published yet, but observing a higher impact of the cathode degradation on the impedance spectrum is in agreement with the results presented by Heins et al.[42] and the reported sensitivity of the cathode to internal resistance changes.[43] Further analysis of the cathode surface isolation shows an unexpected high value at 100 cycles. The low frequency semicircle for 100 cycles has a larger diameter than the upcoming ones which can neither be seen in the Nyquist diagram nor in the analysis in Figure 4 but is revealed by the resulting ageing parameters. We account this result to a temporary decrease of the ambient temperature during this measurement which increases the impedance of the second semicircle. As reported by Heins et al.,[44] the temperature affects the charge transfer semicircle more than the SEI semicircle which could explain why the cathode isolation shows unexpected high values for 100 cycles, while the SEI/electrolyte isolation is unaffected. The last curve shows the loss of active

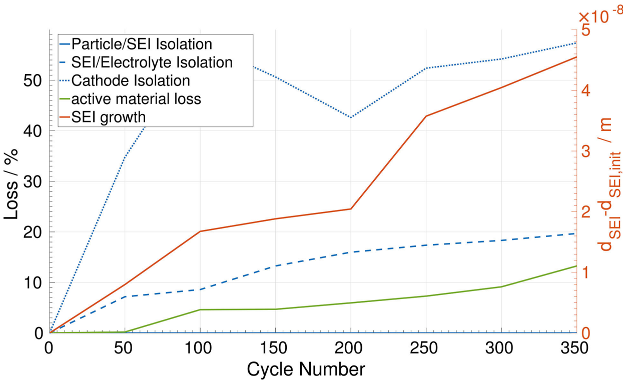

Figure 7. Ageing parameters of the simulated EIS for a cycled Lithium ion battery.

material during cycling following Equation 27. The loss corresponds to the loss of capacity shown in Figure 4. After 350 cycles, approximately 13 % of the anode and cathode active material is assumed to be lost in order to adjust the simulated capacity to the measured value. The percental loss of active material after 350 cycles (13.27 %) is not in complete agreement with the measured percentage loss of the SoH (16.67 %) of the cell until this cycle, because we assume to loose active material at both anode and cathode, while the loss of the limiting electrode has a higher impact on the capacity change. Nevertheless, even if the loss of active material at the two electrodes does not have an equal impact on the capacity and impedance of the cell, it is reported to occur on the anode due to SEI isolations[45–47] and on both electrodes due to particle cracking and loss of connectivity between active material and current collector.[28,48] In conclusion, the values for the identified ageing parameters might not be completely exact, because the newly introduced ageing model has not been validated yet and might not include all relevant ageing processes, but it could be shown, that the chosen set of ageing parameters is not only sufficient to reproduce the measured change in the impedance spectrum but is also in the right order of magnitude and can be reasonably well correlated to physical processes.

4. Conclusions

A physico-chemical single particle battery model has been extended with a new ageing model including a SEI in order to analyse the ageing state of Lithium-ion batteries. Impedance and capacity measurements during cyclic ageing of a NMC/graphite pouch full cell are performed to parameterise the model. Afterwards, parameter identification was conducted on different versions of the introduced ageing model. The study has shown that the model version which assumes SEI growth besides an isolation of the cathode surface is suitable to reproduce the experimentally observed changes in the impedance spectrum as well as the change of the capacity of the cell during ageing. The changes of the high and low frequency semicircles could be attributed to anode and cathode degradation, respectively and the two interfaces facing the electrolyte have been identified to be the decisive factors to reproduce the ageing effects on the impedance spectrum, while the anode/SEI interface has a negligible affect. Furthermore, decreasing quality of the reproduction of the low frequency semicircle close to the end of life indicates additional ageing phenomena not covered by the model. These findings may also be used to predict the EOL of Lithium-ion cells. Although, state estimation for the analysed cell using the introduced ageing model has been successful, model validation with different cells and different cycling conditions has to be done to validate the model assumptions. For future research we suggest to extend the model by P2D characteristics, with a particle size distribution to enable more precise parameter identification by using the impedance instead of the real part of the impedance in the objective function. Cross validation as described and extension of the model with more degradation processes will show if the current model overestimates the values for the SEI thickness and the isolations.

Experimental Section

The pouch-cell used to obtain an exemplary set of experimental data consists of NMC from BASF as cathode and graphite from Hitachi as anode material of a thickness of 71.75 μm and 53.66 μm respectively. Both electrodes have been produced in the Battery LabFactory Braunschweig and been calendered by 10 % resulting in the volume fractions given in Table 3 at a loading of 4.19 $\frac{mg}{cm^2}$ and 9.88 $\frac{mg}{cm^2}$ for anode and cathode respectively. A solvent mixture of EC/DEC with a ratio of 3 : 7 with 1 M $LiPF_6$ as conducting salt and a Celgard 2320 separator have been used. Copper current collector, aluminium current collector and the pouch packaging have been supplied by Somitomo, Hydro and DNP respectively. Electrode and electrolyte parameters used for modelling and simulation are listed

Table 4. Redlich Kister parameters in kJ mol $^{\ 1}$[18].

A_1:	35.80	A_7:	28.79
A_2:	35.01	A_8:	14.98
A_3:	35.25	A_9:	39.91
A_4:	35.69	A_{10}:	96.17
A_5:	38.63	A_{11}:	63.26
A_6:	35.91		

Table 3. Fixed model parameters: (a) measured, (b) calculated according to [43] (c) literature value from, [7] (d) literature value from [18].

Parameter	Anode	Separator	Cathode
Width $\delta/\mu m$	43.66(a)	20.00(a)	56.75(a)
Particle radius $R_i/\mu m$	6.83(a)		6.40(a)
Volume fraction solid ε_s/	0.35(b)		0.33(b)
Volume fraction electrolyte ε_e/	0.60(b)	0.5(b)	0.57(b)
Maximal solid concentration $c_{s,max}/\frac{mol}{m^3}$	28605.42(b)		50862.18(b)
Electrolyte concentration $c_e/\frac{mol}{m^3}$	1000(a)	1000(a)	1000(a)
Transfer coefficients α/	0.50(c)		0.50(c)
Electrolyte phase diffusion coeff. $D_e/\frac{m^2}{s}$	$2.6\cdot10^{\ 10}$(c)	$2.6\cdot10^{\ 10}$(c)	$2.6\cdot10^{\ 10}$(c)
Solid phase diffusion coeff. $D_s/\frac{m^2}{s}$	$2.0\cdot10^{\ 16}$(c)		$3.7\cdot10^{\ 16}$(c)
Transference number t_p/	0.37(c)		0.37(c)
Bruggeman's exponent β/	1.50(c)	1.50(c)	1.50(c)
Reaction rate constant $k_{f,a}/\frac{m^{2\ 5}}{mol^{0\ 5}s}$	$10^{\ 7}$(d)		
Redlich Kister Parameters			

in Table 3. A discharge at the Beginning Of Life (BOL) with $C/20$ yielded a capacity of 28.28 mAh for a given electrode area of 24.95 cm^2. All impedance measurements were performed with a Zahner Electrochemical Workstation (Zennium E) in galvanostatic modus at SoC 50. The frequency range was set between 20 mHz and 5 MHz, discretised with ten frequencies per decade above 66 Hz and five frequencies per decade for frequencies below 66 Hz. For the EIS, an amplitude of $C/15$ was used. The cycling procedure included charging with 1 C constant current until 4.2 V and an additional constant voltage step until the current decreases below $C/20$. Discharge was performed with 1 C constant current until 2.9 V. The capacity of the cell has been calculated using the last charging routine prior to each impedance measurement. With the actual capacity and the nominal capacity at the BOL, the SoH of the cell was determined. A SoH of 100 is equivalent to a measured capacity of 28.39 mAh at 0 cycles. Previous to the first impedance measurement at 0 cycles two activation cycles have been used to activate the cell. Every 50 cycles of charge/discharge, after an idle time of 10 min to ensure steady state conditions, an impedance spectrum was measured. The measurement procedure was performed at an environmental temperature of 25 °C. Only one cell is tested to gain experimental data from a well known cell. No comparison with different cycling conditions have been done since the scope of this work ends with the introduction of the novel ageing model and the state estimation of the used cell.

Acknowledgements

We thank for the support from Battery LabFactory Braunschweig.

Conflict of Interest

The authors declare no conflict of interest.

Keywords: double layer · electrochemical impedance spectroscopy · graphite · lithium-ion batteries · nickel manganese cobalt oxide

[1] P. B. Balbuena, Y. Wang, *Lithium Ion Batteries Solid Electrolyte Interphase*, Imperial College Press, London, **2004**.
[2] D. Aurbach, B. Markovsky, I. Weissman, E. Levi, Y. Ein Eli, *Electrochim. Acta* **1999**, *45*, 67 86.
[3] N. Harting, N. Wolff, F. Röder, U. Krewer, *Electrochim. Acta* **2017**, *248* 133 139.
[4] N. Wolff, N. Harting, M. Heinrich, F. Röder, U. Krewer, *Electrochim. Acta* **2018**, *260*, 614 622.
[5] M. Doyle, F. Fuller, J. Newman, *J. Electrochem. Soc.* **1993**, *140*, 1526.
[6] I. Ong, J. Newman, *J. Electrochem. Soc.* **1999**, *146*, 4360.
[7] N. Legrand, S. Raël, B. Knosp, M. Hinaje, P. Desprez, F. Lapicque, *J. Power Sources* **2014**, *251*, 370 378.
[8] E. Peled, D. Golodnitsky, G. Ardel, V. Eshkenazy, *Electrochim. Acta* **1995**, *40*, 2197 2204.
[9] L. Gao, D. Macdonald, *J. Electrochem. Soc.* **1997**, *144*, 1174 1179.
[10] D. Macdonald, *J. Electrochem. Soc.* **1992**, *139*, 3434.
[11] I. Nainville, A. Lemarchand, J. P. Badiali, *Electrochim. Acta* **1996**, *41*, 2855 2863.
[12] M. Broussely, S. Herreyre, P. Biensan, P. Kasztejna, K. Nechev, R. J. Staniewicz, *J. Power Sources* **2001**, *97 98*, 13 21.
[13] J. Christensen, J. Newman, *J. Electrochem. Soc.* **2004**, *151*, A1977.
[14] P. Ramadass, B. Haran, R. White, B. N. Popov, *J. Power Sources* **2003**, *123*, 230 240.
[15] P. Ramadass, B. Haran, P. M. Gomadam, R. White, B. N. Popov, *J. Electrochem. Soc.* **2004**, *151*, A196.
[16] G. Ning, B. N. Popov, *J. Electrochem. Soc.* **2004**, *151*, A1584.
[17] A. Colclasure, R. Kee, *Electrochim. Acta* **2010**, *55*, 8960 8973.
[18] A. Colclasure, K. Smith, R. Kee, *Electrochim. Acta* **2011**, *58*, 33 43.
[19] F. Röder, R. D. Braatz, U. Krewer, *J. Electrochem. Soc.* **2017**, *164*, E3335 E3344.
[20] T. Zavalis, M. Klett, M. Kjell, M. Behm, R. Lindström, G. Lindbergh, *Electrochim. Acta* **2013**, *110*, 335 348.
[21] Y. Xie, J. Li, C. Yuan, *Electrochim. Acta* **2014**, *127*, 266 275.
[22] J. P. Meyers, M. Doyle, R. M. Darling, J. Newman, *J. Electrochem. Soc.* **2000**, *147*, 2930.
[23] J. Newman, *Electrochemical Systems*, John Wiley and Sons, Hoboken, **2004**.
[24] M. R. Busche, T. Drossel, T. Leichtweiss, D. A. Weber, M. Falk, M. Schneider, M. L. Reich, H. Sommer, P. Adelhelm, J. Janek, *Nat. Chem.* **2016**, *8*, 426 434.
[25] Y. Yamada, F. Sagane, Y. Iriyama, T. Abe, Z. Ogumi, *J. Phys. Chem. C* **2009**, *113*, 14528 14532.
[26] F. G. Helfferich, *Comprehensive Chemical Kinetics Kinetics of Homogeneous Multistep Reactions.*, (Eds.: R. G. Compton, G. Hancock), Elsevier, London, **2001**, 164 165.
[27] Y. Kitazumi, O. Shirai, M. Yamamoto, K. Kano, *Electrochim. Acta* **2018**, *259*, 542 551.
[28] P. Arora, R. E. White, M. Doyle, *J. Electrochem. Soc.* **1998**, *145*, 3647.
[29] M. Broussely, P. Biensan, F. Bonhomme, P. Blanchard, S. Herreyre, K. Nechev, R. J. Staniewicz, *J. Power Sources* **2005**, *146*, 90 96.
[30] M. Koltypin, D. Aurbach, L. Nazar, B. Ellis, *J. Power Sources* **2007**, *174*, 1241 1250.
[31] U. Tröltzsch, O. Kanoun, H. R. Tränkler, *Electrochim. Acta* **2006**, *51*, 1664 1672.
[32] S. Tippmann, D. Walper, L. Balboa, B. Spier, W. G. Bessler, *J. Power Sources* **2014**, *252*, 305 316.
[33] S. M. M. Alavi, C. R. Birkl, D. A. Howey, *J. Power Sources* **2015**, *288*, 345 352.
[34] J. Illig, J. P. Schmidt, M. Weiss, A. Weber, E. Ivers Tiffée, *J. Power Sources* **2013**, *239*, 670 679.
[35] J. Huang, Z. Li, J. Zhang, S. Song, Z. Lou, N. Wu, *J. Electrochem. Soc.* **2015**, *162*, A585 A595.
[36] C. Gabrielli, *Tech. Rep.* **1984**, 004/84.
[37] D. P. Abraham, J. L. Knuth, D. W. Dees, I. Bloom, J. P. Christophersen, *J. Power Sources* **2007**, *170*, 465 475.
[38] D. P. Abraham, S. D. Poppen, A. N. Jansen, J. Liu, D. W. Dees, *Electrochim. Acta* **2004**, *49*, 4763 4775.
[39] A. Andersson, A. Henningson, H. Siegbahn, U. Jansson, K. Edström, *J. Power Sources* **2003**, *119 121*, 522 527.
[40] M. Nie, D. Chalasani, D. Abraham, Y. Chen, A. Bose, B. Lucht, *J. Phys. Chem. C* **2013**, *117*, 1257 1267.
[41] S. Shi, Y. Qi, H. Li, L. Hector, *J. Phys. Chem. C* **2013**, *117*, 8579 8593.
[42] T. P. Heins, N. Schlüter, U. Schröder, *ChemElectroChem* **2017**, *4*, 2921 2927.
[43] G. Lenze, F. R"oder, H. Bockholt, W. Haselrieder, A. Kwade, U. Krewer, *J. Electrochem. Soc.* **2017**, *164*, A1223 A1233.
[44] T. P. Heins, N. Harms, L. S. Schramm, U. Schröder, *Energy Technol.* **2016**, *4*, 1 6.
[45] G. Sikha, B. N. Popov, R. E. White, *J. Electrochem. Soc.* **2004**, *151*, A1104.
[46] R. Fu, S. Y. Choe, V. Agubra, J. Fergus, *J. Power Sources* **2014**, *261*, 120 135.
[47] D. Aurbach, M. D. Levi, E. Levi, A. Schechter, *J. Phys. Chem. B* **1997**, *101*, 2195 2206.
[48] L. Shi, U. Kunz, *Energy Technol.* **2016**, *4*, 1520 1530.